Unraveling amino acid residues critical for allosteric potentiation of (α4)3(β2)2-type nicotinic acetylcholine receptor responses

Received for publication, December 5, 2016, and in revised form, April 20, 2017 Published, Papers in Press, April 26, 2017, DOI 10.1074/jbc.M116.771246

Ze-Jun Wang[‡1], Farah Deba[‡1], Tasnim S. Mohamed[‡], David C. Chiara[§], Kara Ramos[‡], and Ayman K. Hamouda[‡¶2]

From the [‡]Department of Pharmaceutical Sciences, Texas A&M Health Sciences Center, Kingsville, Texas 78363, [¶]Department of Neuroscience and Experimental Therapeutics, Texas A&M Health Sciences Center, Bryan, Texas 77807, and [§]Department of Neurobiology, Harvard Medical School, Boston, Massachusetts 02115

Edited by F. Anne Stephenson

Neuronal nicotinic acetylcholine receptors (nAChRs) are promising drug targets to manage several neurological disorders and nicotine addiction. Growing evidence indicates that positive allosteric modulators of nAChRs improve pharmacological specificity by binding to unique sites present only in a subpopulation of nAChRs. Furthermore, nAChR positive allosteric modulators such as NS9283 and CMPI have been shown to potentiate responses of (α4)3(β2)2 but not (α4)2(β2)3 nAChR isoforms. This selective potentiation underlines that the α4:α4 interface, which is present only in the (α4)3(β2)2 nAChR, is an important and promising drug target. In this report we used site-directed mutagenesis to substitute specific amino acid residues and computational analyses to elucidate CMPI's binding mode at the α4:α4 subunit extracellular interface and identified a unique set of amino acid residues that determined its affinity. We found that amino acid residues α4Gly-41, α4Lys-64, and α4Thr-66 were critical for (α4)3(β2)2 nAChR potentiation by CMPI, but not by NS9283, whereas amino acid substitution at α4His-116, a known determinant of NS9283 and of agonist binding at the α4:α4 subunit interface, did not reduce CMPI potentiation. In contrast, substitutions at α4Gln-124 and α4Thr-126 reduced potentiation by CMPI and NS9283, indicating that their binding sites partially overlap. These results delineate the role of amino acid residues contributing to the α4:α4 subunit extracellular interface in nAChR potentiation. These findings also provide structural information that will facilitate the structure-based design of novel therapeutics that target selectively the (α4)3(β2)2 nAChR.

Drugs that enhance the function of brain nicotinic acetylcholine receptors (nAChRs)[3] are sought for their potential clinical applications in the management of nicotine dependence (tobacco smoking) and for improvement of cognitive deficits associated with neurological and psychiatric disorders (1). However, it has proven challenging to develop nAChR therapeutics selective for nAChR subtypes, and few are available clinically (2). Neuronal nAChRs are transmitter (ACh)-gated ion channels made up of five homologous or identical subunits (α2-α9 and β2-β4), each one consisting of a large N-terminal extracellular domain and a 4-helix bundle transmembrane domain. The recently published X-ray structure of (α4)2(β2)3 nAChR confirmed this general subunit topology and provided further insight into the 3D structure of neuronal nAChRs (3). Whereas there are multiple neuronal nAChR subtypes with unique pathophysiological and pharmacological profiles, the α4- and β2-containing nAChR subtypes are of particular interest (4, 5). They constitute the majority of brain nAChRs (6) and are the primary nAChR subtypes that mediate the addictive effects of nicotine (7, 8). In addition, they are important for neuronal survival and maintenance of cognitive performance and learning during aging (9), and there is a decrease in their number in the brain of Alzheimer's patients (10).

Drugs that enhance signaling through nAChRs include agonists and partial agonists that bind to the orthosteric (ACh) binding sites and directly activate the nAChR and positive allosteric modulators (PAM) that enhance ACh potency and/or efficacy by binding at sites distinct from the ACh-binding sites (11). Many years of effort have defined the ACh-binding sites at subunit interfaces within the extracellular domain and determined structural requirements for nAChR agonists (12). In contrast, compounds with diverse structural features potentiate nAChRs (1), and multiple PAM recognition sites have been proposed. These include pockets at the extracellular canonical (agonist-binding) and non-canonical subunit interfaces (13–17), within the transmembrane domain in the helix bundle of a single subunit (18), at the interface between adjacent subunits (19), and at the subunit's extracellular C-tail (20–21). There is

This work was supported, in whole or in part, by National Institutes of Health Grant NS-093590 (NINDS; to A. K. H.). This work was also supported in part by Faculty Development Fund of Texas A&M Health Sciences Center (to A. K. H.). The authors declare that they have no conflicts of interest with the contents of this article. The content is solely the responsibility of the authors and does not necessarily represent the official views of the National Institutes of Health.

[1] Both authors contributed equally to this work.

[2] To whom correspondence should be addressed: Dept. of Pharmaceutical Sciences, Rangel College of Pharmacy, Texas A&M Health Sciences Center, Kingsville, TX 78363. Tel.: 361-221-0750; Fax: 361-221-0793; E-mail: Hamouda@tamhsc.edu.

[3] The abbreviations used are: nAChR, nicotinic acetylcholine receptor; ACh, acetylcholine; AChBP, acetylcholine-binding protein; CMPI, 3-(2-chlorophenyl)-5-(5-methyl-1-(piperidin-4-yl)-1H-pyrrazol-4-yl)isoxazole; dFBr, desformylflustrabromine; PAM, positive allosteric modulator; NS9283, 3-[3-(pyridin-3-yl)-1,2,4-oxadiazol-5-yl]benzonitrile.

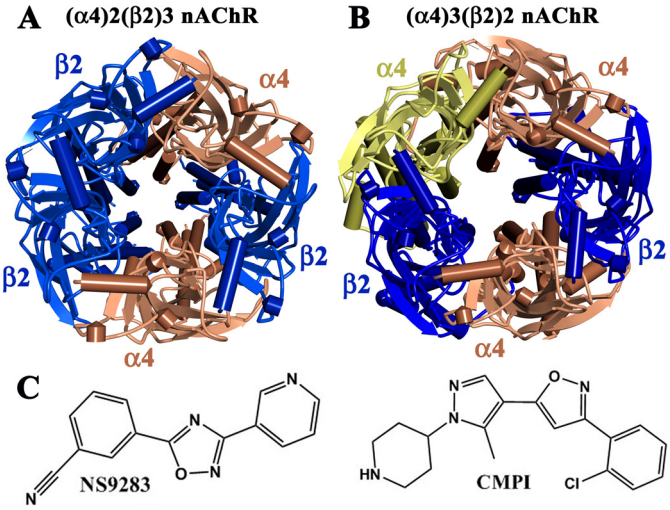

Figure 1. *A*, top view of the X-ray structure of human (α4)2(β2)3 nAChRs (PDB accession number 5KXI). *B*, top view of a homology model of an $(\alpha4)_3(\beta2)_2$ nAChR based on the crystal structure of (α4)2(β2)3 nAChRs. *C*, chemical structure of nAChRs PAMs: NS9283 and CMPI.

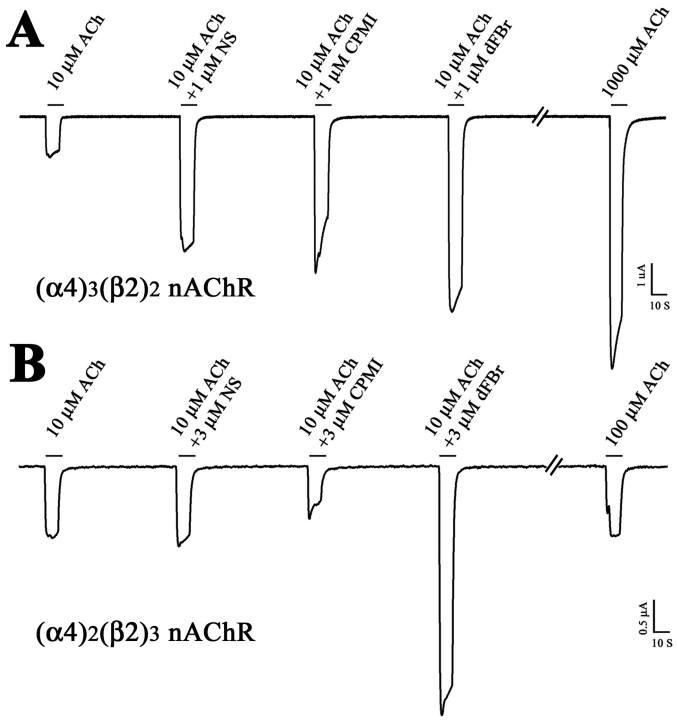

Figure 2. Representative traces showing the effects of CMPI, NS9283, and dFBr on ACh-induced current responses of (α4)3(β2)2 (*A*) and (α4)2(β2)3 (*B*) nAChRs, respectively. *Xenopus* oocytes expressing wild type human (α4)3(β2)2 or (α4)2(β2)3 nAChRs were voltage-clamped at −50 mV, and currents elicited by 10-s applications of 10 μM ACh were recorded in the absence or presence of 1 or 3 μM CMPI, NS9283, or dFBr.

an increasing interest in the development of novel nAChR PAMs, as they provide potentially selective modulation of a subpopulation of nAChRs while avoiding the sustained receptor activation and non-physiological alteration in cholinergic transmission seen with agonists (11, 22).

Neuronal nAChRs consisting of the α4 and β2 subunits, alone or with additional nAChR subunits, exist in two pharmacologically distinct isoforms (Fig. 1. *A* and *B*) (23–24). The (α4)2(β2)3 nAChR exhibits high sensitivity for ACh and other nAChR agonists (ACh EC_{50} ~1 μM), whereas the (α4)3(β2)2 nAChR has lower sensitivity for ACh and other nAChR agonists (ACh EC_{50} ~100 μM). Although both isoforms have ACh-binding sites at the two agonist-binding "canonical" α4:β2 extracellular interfaces, recent findings establish the presence of a low-affinity ACh-binding site within the "non-canonical" α4:α4 extracellular interface, which is present only in the (α4)3(β2)2 nAChR isoform (25–27). In addition to altering agonist sensitivity, the α4:α4 subunit interface in the (α4)3(β2)2 nAChR confers selectivity to nAChR PAMs (28–30).

Here, we expand these studies to identify the amino acid residues at the α4:α4 subunit interface that are important for (α4)3(β2)2 nAChR potentiation by CMPI (Fig. 1*C*; 3-(2-chlorophenyl)-5-(5-methyl-1-(piperidin-4-yl)-1H-pyrrazol-4-yl)isoxazole), a potent nAChR PAM that potentiates (α4)3(β2)2 but not (α4)2(β2)3 nAChR (30, 31). We express (α4)3(β2)2 nAChR, wild-type or containing amino acid substitutions, in *Xenopus laevis* oocytes and use two-electrode voltage-clamp recordings to assess the effect of these substitutions on (α4)3(β2)2 nAChR modulation by CMPI, NS9283 (3-[3-(pyridin-3-yl)-1,2,4-oxadiazol-5-yl]benzonitrile, another PAM that also requires the presence of α4:α4 interface for potentiation; Refs. 17 and 32), and desformylflustrabromine (dFBr, a PAM of (α4)3(β2)2 and (α4)2(β2)3 nAChRs (33, 34)).

Results

Previous studies have established dFBr, CMPI, and NS9283 as potent nAChR PAMs with high selectivity for the α4-containing nAChRs (28, 31, 35). In addition, the effects of dFBr, CMPI and NS9283 on high- and low-agonist sensitivity isoforms of α4β2 nAChR have been examined by recording ACh-induced currents from *Xenopus* oocytes injected with α4 and β2 subunits RNAs at ratios that favor the expression of (α4)3(β2)2 or (α4)2(β2)3 nAChR. dFBr potentiated both α4β2 nAChR isoforms, whereas NS9283 and CMPI potentiated (α4)3(β2)2 (low sensitivity) nAChR but not (α4)2(β2)3 (high sensitivity) nAChR (17, 30). As shown in Fig. 2*A*, co-application of 1 μM CMPI, NS9283, or dFBr with ACh enhanced ACh-induced current responses of *Xenopus* oocytes expressing (α4)3(β2)2 nAChR. In contrast, ACh-induced current responses of (α4)2(β2)3 nAChR were enhanced by co-application of dFBr but not CMPI or NS9283 (Fig. 2*B*). Coapplication of CMPI or NS9283 at concentrations up to 10 μM did not enhance (α4)2(β2)3 nAChR current responses to 1, 3, or 10 μM ACh (data not shown).

Effect of amino acid substitutions at the α4:α4 subunit extracellular interface on modulation by CMPI

The stoichiometry dependence of enhancement by NS9283 and CMPI underscores an essential role in nAChR allosteric modulation of the non-canonical α4:α4 subunit interface, which is present only in the (α4)3(β2)2 nAChR. It also indicates the presence of at least two classes of PAM-binding sites within the α4β2 nAChR: one (or more) at the α4:α4 subunit interface that mediates the effect of NS9283 and CMPI and one (or more) at the α4:β2 and/or β2:α4 subunit interfaces that mediates the effect of dFBr. Indeed, a histidine-to-valine substitution at posi-

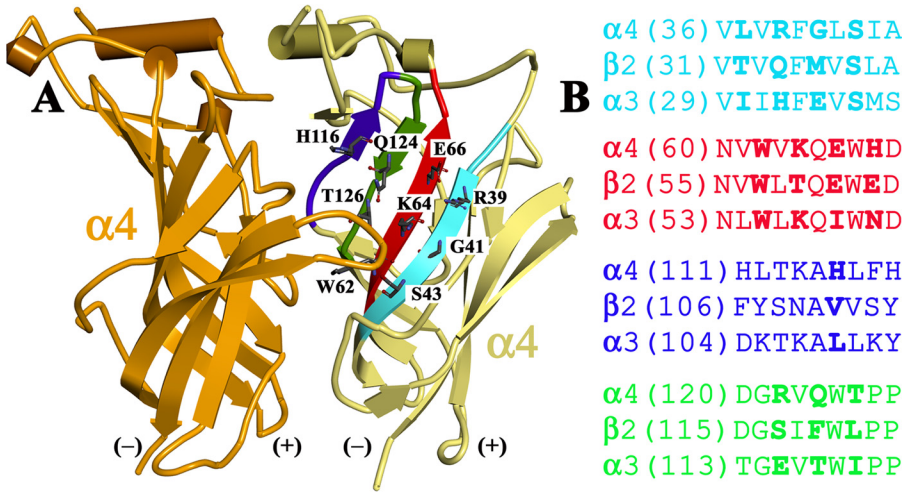

Figure 3. *A*, side view of a homology model of an (α4)3(β2)2 nAChR showing amino acid residues contributing to the α4(−) face of the α4:α4 extracellular interface. *B*, sequence alignments of amino acid contributing to the (−) face of the interface with corresponding regions in the β2 and α3 nAChR subunits. Amino acid numbering is for mature protein according to the X-ray structure of human (α4)2(β2)3 nAChRs (PDB accession number 5KXI). Add 26, 25, and 31 to α4, β2, and α3 sequence numbers, respectively, to obtain amino acid numbers starting from the translational N terminus. β-Strands in *A* are color-coded (β1, *cyan*; β2, *red*; β5, *blue*; β6, *green*) to match their sequence alignments in *B*.

tion α4His-116 (α4His-142 when numbering includes the signal peptide), which projects into the α4:α4 subunit extracellular interface, significantly reduced NS9283 potentiation of (α4)3(β2)2 nAChRs (32). Because CMPI does not potentiate (α4)2(β2)3 or (α3)3(β2)2 nAChR, we reasoned that amino acid substitutions making the α4 subunit more similar to the α3 or β2 subunit will lead to identification of amino acid residues that confer CMPI selectivity to (α4)3(β2)2 nAChR and test the possibility that NS9283 and CMPI share the same determinants for potentiation.

The non-canonical α4:α4 subunit extracellular interface is made up of amino acid residues from a (+) face of one α4 subunit and a (−) face of the adjacent α4 subunit. The α4 subunit (+) face is also present at the canonical α4:β2 interface where it provides the core aromatic residues of the agonist-binding sites, whereas the α4 subunit (−) face is also at the β2:α4 interface present in the (α4)2(β2)3 and (α4)3(β2)2 nAChRs. Based on amino acid sequence alignments of α4, β2, and α3 subunits and a homology model of the (α4)3(β2)2 nAChR (Fig. 3), 10 non-conserved amino acid residues within the α4 subunit (−) face that project into the α4:α4 extracellular interface were identified and substituted to the corresponding amino acid residues in the β2 and/or α3 subunit.

The effects of these amino acid substitutions were assessed by recording ACh-induced current responses (± CMPI, NS9283, or dFBr) of *Xenopus* oocytes injected with a mix of RNA encoding α4 containing the point mutation and WT β2 subunit RNA at a ratio of 8:1 to favor the expression of the 3α4:2β2 stoichiometry (Fig. 4*A*). The potentiation for each amino acid substitution was determined as *R*, the ratio of the peak current amplitude in the presence of 1 μM PAM and 10 μM ACh (EC_{10}) relative to the peak current amplitude elicited by 10 μM ACh alone (Table 1). Consistent with previous reports (17, 32), valine substitution at α4His-116 (α4H116V) abolished the enhancement by 1 μM NS9283 (R_{H116V} = 1.1 ± 0.1 *versus* R_{WT} = 3.8 ± 0.3). In contrast, the α4H116V substitution did not reduce enhancement by CMPI (R_{H116V} = 5.3 ± 0.4 *versus* R_{WT} = 4.3 ± 0.4) or dFBr (R_{H116V} = 5.9 ± 0.4 *versus* R_{WT} = 5.1 ± 0.4). Similar effects were seen for CMPI in receptors harboring α4H116L or α4H116A substitutions (Table 1), which indicates that the position α4His-116 is not essential for CMPI or dFBr modulation of (α4)3(β2)2 nAChR.

In contrast to α4His-116, for (α4)3(β2)2 nAChRs containing α4G41M, α4K64T, or α4E66I mutant subunits, potentiation by NS9283 was unaffected, whereas potentiation by CMPI was reduced to <1.5-fold that for 10 μM ACh alone (Table 1). These results establish a selective role of α4Gly-41, α4Lys-64, and α4Glu-66 in CMPI potentiation of the (α4)3(β2)2 nAChR.

The substitution α4Q124T reduced potentiation by either CMPI or NS9283 at 1 μM to ~2 and 1.6, respectively, whereas the substitution α4T126I reduced potentiation to ~1.2 and 1, respectively. However, at 10 μM, NS9283, but not CMPI, potentiated ACh current responses of (α4Q124F)3(β2)2 and (α4T126L)3(β2)2 nAChRs by 4.3 ± 0.2- and 1.73 ± 0.1-fold, respectively (Fig. 4*B*). Thus, positions α4Gln-124 and α4Thr-126 contribute to (α4)3(β2)2 nAChR potentiation by CMPI and NS9283 but are more important for CMPI than NS9283.

Amino acid substitutions at positions α4Leu-37, α4Arg-39, α4His-68, and α4Arg-122 had no significant effect ($p < 0.001$) on CMPI or NS9283 potentiation (Table 1), indicating a minimal role, if any, of these amino acid residues in CMPI or NS9283 potentiation of (α4)3(β2)2 nAChR. None of the tested amino acid substitutions within the α4(−) extracellular interface had a significant effect on dFBr potentiation of (α4)3(β2)2 nAChR (Table 1).

Effect of amino acid substitutions in the transmembrane domain on modulation by CMPI

Within the transmembrane domain, the α4:α4 subunit interface is formed by amino acid residues from the M3 helix of the α4 subunit providing the (+) face and residues from the M1 helix of the α4 subunit providing the (−) face as well as amino acid residues from M2 of both subunits. The α4 and α3 subunits share high amino acid sequence identity within M1-M2-M3,

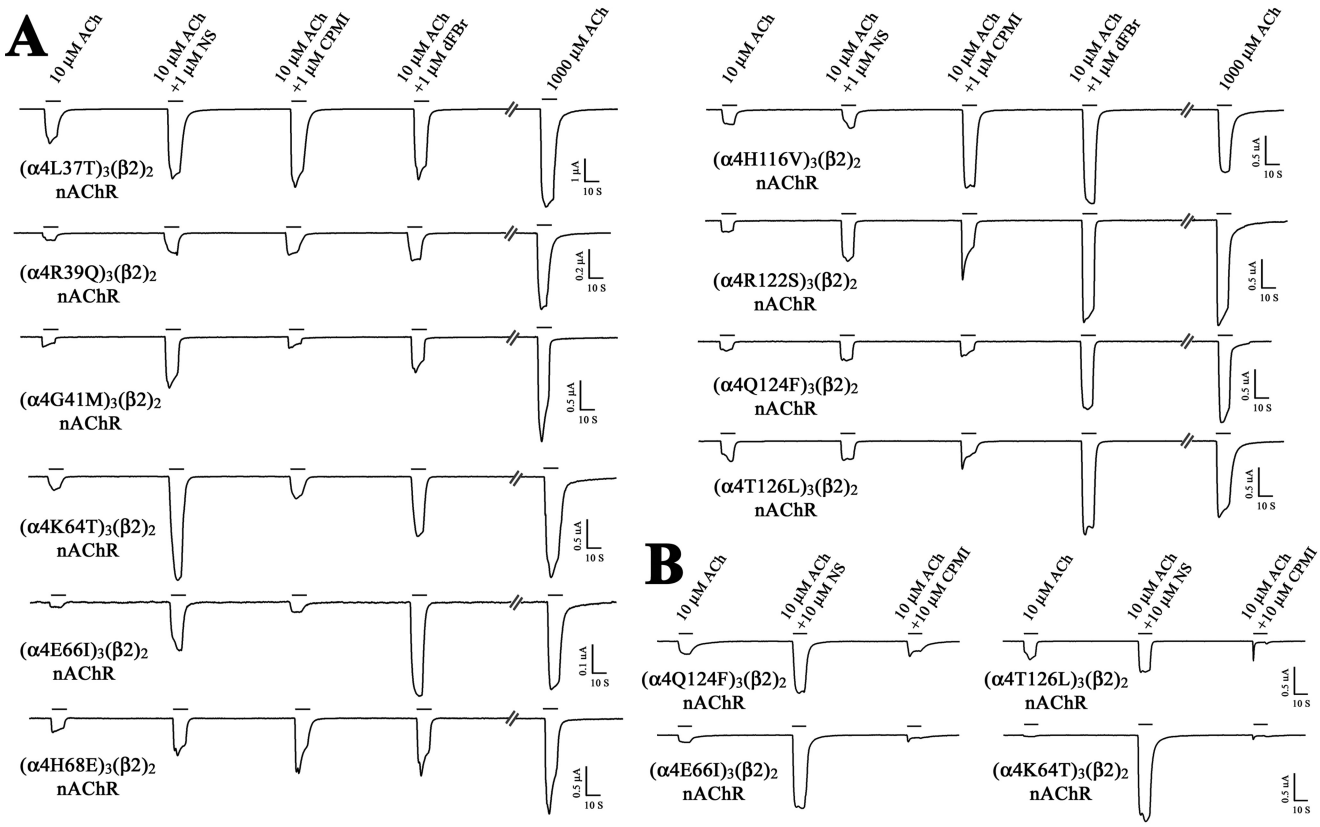

Figure 4. Effect of amino acid substitutions on CMPI, NS9283, and dFBr potentiation of (α4)3(β2)2 nAChRs. Representative two-electrode voltage clamp traces showing the effects of 1 μM CMPI, NS9283 or dFBr (*A*) and 10 μM CMPI or NS9283 (*B*) on ACh-induced current responses of *Xenopus* oocytes expressing WT or mutant (α4)3(β2)2 nAChRs containing an amino acid substitution at the (−) face of the α4 subunit. Quantification of CMPI, NS9283, and dFBr effects are presented in Table 1.

Table 1

Modulation of WT and mutant (α4)3(β2)2 nAChRs by NS9283, CMPI, and dFBr

Current responses to 10 μM ACh, 10 μM ACh +1 μM NS9283, 10 μM ACh +1 μM CMPI, 10 μM ACh +1 μM dFBr, and 1 mM ACh were recorded from oocytes expressing WT and mutant (α4)3(β2)2 nAChRs (Fig. 4). -Fold potentiation in the presence of various PAMs was calculated as *R*, the ratio of peak current amplitude in the presence of 1 μM PAM relative to peak current amplitude elicited by 10 μM ACh alone from the same recording run. Replicas from the same oocyte were averaged. The data in the table are the average (Avg) ± S.E. of several oocytes (*N*). The probability (*P*) that -fold potentiation differs from no potentiation (10 μM ACh+PAM/10 μM ACh = 1) was analyzed using one-way analysis of variance with the Holm-Sidak test (SigmaPlot, Systat Software Inc.). *R*(NS9283), *R*(CMPI), and *R*(dFBr) values calculated for high sensitivity (α4)2(β2)3 nAChRs ($n = 4$) were 1.0 ± 0.1, 0.8 ± 0.1, and 2.5 ± 0.5, respectively.

	R(NS9283)			*R*(CMPI)			*R*(dFBr)			ACh (1 mM/10 μM)	
Combination	Ave ± S.E.	*N*	*P*	Ave ± S.E.	*N*	P	Ave ± S.E.	*N*	*P*	Ave ± S.E.	*N*
α4:β2	3.8 ± 0.3	23	<0.001	4.3 ± 0.3	23	<0.001	5.1 ± 0.4	23	<0.001	8.8 ± 1.1	23
α4L37I:β2	3.8 ± 0.2	5	<0.001	4.6 ± 0.4	9	<0.001	3.5 ± 0.3	5	<0.001	10.0 ± 1.4	5
α4L37T:β2	3.3 ± 0.4	5	<0.001	3.7 ± 0.3	10	<0.001	3.7 ± 0.3	5	<0.001	7.9 ± 1.0	8
α4R39Q:β2	3.5 ± 0.2	3	<0.001	3.7 ± 0.4	7	<0.001	5.2 ± 0.4	3	<0.001	7.6 ± 0.7	10
α4R39H:β2	4.6 ± 0.2	3	<0.001	4.6 ± 0.5	7	<0.001	5.3 ± 1.8	3	<0.001	12.2 ± 1.0	4
α4G41M:β2	4.1 ± 0.7	3	<0.001	1.2 ± 0.1	6	0.664	3.3 ± 0.2	3	0.011	7.9 ± 1.1	7
α4G41E:β2	3.9 ± 0.4	6	<0.001	1.7 ± 0.2	11	0.023	4.1 ± 0.2	6	<0.001	10.8 ± 1.7	8
α4K64T:β2	7.4 ± 0.3	4	<0.001	1.4 ± 0.1	8	0.186	4.2 ± 0.3	4	<0.001	8.1 ± 0.6	7
α4E66I:β2	5.6 ± 0.4	6	<0.001	1.2 ± 0.1	10	0.564	9.3 ± 1.8	7	<0.001	10.0 ± 1.1	10
α4H68N:β2	4.8 ± 0.3	7	<0.001	4.7 ± 0.3	10	<0.001	5.8 ± 0.5	7	<0.001	8.7 ± 0.7	10
α4H68E:β2	3.0 ± 0.5	5	<0.001	4.0 ± 0.5	8	<0.001	5.5 ± 1.1	5	<0.001	8.5 ± 1.0	9
α4H116V:β2	1.1 ± 0.1	4	0.718	5.3 ± 0.4	8	<0.001	5.9 ± 0.4	4	<0.001	7.8 ± 0.9	8
α4H116L:β2	1.6 ± 0.2	5	0.200	3.1 ± 0.3	9	<0.001	8.1 ± 0.6	5	<0.001	12 ± 2.2	8
α4H116A:β2	1.3 ± 0.2	3	0.426	7.6 ± 0.4	6	<0.001	8.1 ± 0.9	3	<0.001	11.2 ± 2.4	5
α4R122S:β2	2.9 ± 0.4	4	<0.001	4.0 ± 0.7	8	<0.001	8.0 ± 2.2	5	<0.001	11.3 ± 1.4	9
α4R122E: β2	3.0 ± 0.2	4	<0.001	3.6 ± 0.3	8	<0.001	10.3 ± 2.4	5	<0.001	15.9 ± 2.5	9
α4Q124T:β2	2.0 ± 0.1	6	0.001	1.6 ± 0.1	9	0.051	3.9 ± 0.1	6	<0.001	4.9 ± 0.2	9
α4Q124F:β2	1.8 ± 0.1	4	0.034	1.4 ± 0.1	11	0.255	6.3 ± 0.8	4	<0.001	8.2 ± 1.0	9
α4T126L:β2	1.3 ± 0.2	3	0.496	1.3 ± 0.1	7	0.460	5.1 ± 0.6	4	<0.001	3.3 ± 0.5	9
α4T126I:β2	1.3 ± 0.1	8	0.252	0.7 ± 0.1	10	0.448	2.6 ± 0.4	8	0.004	2.3 ± 0.5	15
α4C233F:β2	3.0 ± 0.4	5	<0.001	2.9 ± 0.2	5	<0.001	3.1 ± 0.3	5	<0.001	4.8 ± 0.4	5
α4I249V:β2	2.5 ± 0.1	4	<0.001	3.0 ± 0.4	4	<0.001	4.1 ± 0.6	4	<0.001	5.8 ± 0.9	4
α4L265V:β2	3.1 ± 0.4	3	<0.001	3.8 ± 0.4	3	<0.001	3.2 ± 0.1	3	<0.001	6.5 ± 1.1	3
α4H306Y:β2	2.4 ± 0.1	3	<0.001	5.1 ± 0.1	3	<0.001	5.9 ± 0.3	3	<0.001	11 ± 0.7	3

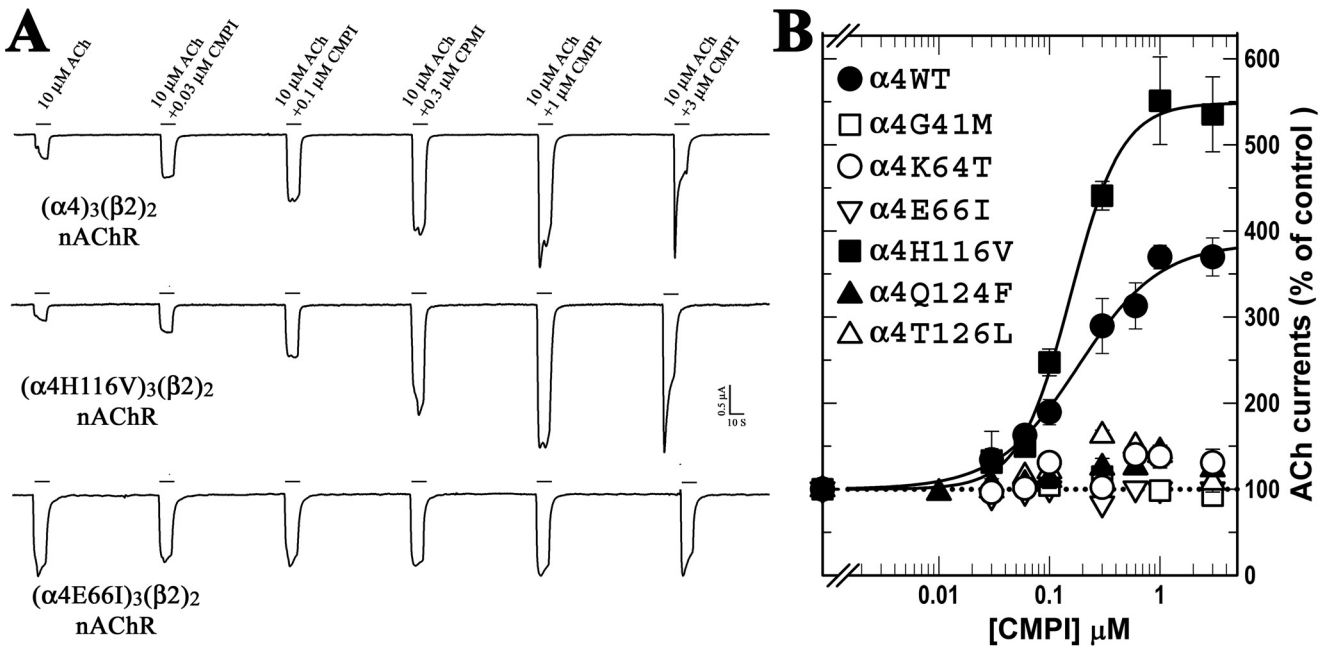

Figure 5. CMPI concentration-dependent potentiation of WT and mutant (α4)3(β2)2 nAChRs. *A*, representative two-electrode voltage clamp traces showing the effect of increasing concentrations of CMPI on ACh-induced current responses of *Xenopus* oocytes expressing WT or mutant (α4)3(β2)2 nAChRs containing amino acid substitutions at the (−)face of α4 subunit. *B*, for each recording run, peak currents were normalized to the peak current elicited by 10 μM ACh alone, replicas from individual oocytes were averaged, and the average ± S.E. of data from several oocytes were plotted and fit (when possible) to a single-site model using Equation 1. Parameters (potentiation EC_{50} and I_{max}) are shown in Table 2.

differing by one amino acid in M1 (α4Cys-233), three amino acid residues in M2 (α4Ile-249, α4Leu-265, and α4Ile-269), and one toward the cytoplasmic end of M3 (α4His-306). Amino acid substitutions at positions α4Cys-233, α4Ile-249, α4Leu-265, and α4His-306 to the corresponding amino acid residues in the α3 subunit had no significant effect ($p < 0.001$) on CMPI or NS9283 potentiation (Table 1).

CMPI concentration-dependent potentiation of WT and mutant (α4)3(β2)2 nAChRs

In WT (α4)3(β2)2 nAChR, co-application of CMPI maximally potentiated ACh current responses by ~400% with an EC_{50} of ~0.3 μM (30). We examined the effect of amino acid substitutions at the α4:α4 extracellular interface on the concentration dependence of CMPI potentiation by recording current responses to 10 μM ACh (EC_{10}) alone or in the presence of increasing concentrations of CMPI on oocytes expressing WT and mutant (α4)3(β2)2 nAChRs (Fig. 5). For WT (α4)3(β2)2 nAChR, CMPI produced a maximal potentiation (I_{max}) of 386 ± 15% with an EC_{50} of 0.18 ± 0.03 μM (Table 2). For (α4)3(β2)2 nAChRs containing amino acid substitutions at positions α4Gly-41, α4Lys-64, α4Glu-66, α4Gln-124, or α4Thr-126, the observed current responses to 10 μM ACh in the presence of CMPI at any concentration tested (0.01–3 μM) was not significantly different from no CMPI (Table 2). In contrast, for (α4)3(β2)2 nAChRs containing amino acid substitutions at positions α4Leu-37, α4Gln-39, α4His-68, α4His-116, or α4Arg-122, the values of I_{max} for CMPI potentiation were significantly different from no CMPI ($p < 0.001$; Table 2). Indeed, the substitutions α4L37I, α4R39H, α4H116V, and α4H116V resulted in a higher CMPI I_{max} than seen for WT. The CMPI EC_{50} values for these mutants were not significantly different from that for WT (α4)3(β2)2 nAChR, consistent with no effect of amino acid substitution at α4Leu-37, α4Gln-39, α4His-68, α4His-116, or α4Arg-122 on the potency of CMPI as (α4)3(β2)2 nAChR potentiator.

The effect of CMPI on ACh concentration-response curves of WT and mutant (α4)3(β2)2 nAChRs

Recent reports support the presence of a low-affinity ACh-binding site at the α4:α4 subunit extracellular interface with substitutions of amino acid residues contributing to the α4:α4 subunit extracellular interface altering the ACh concentration-response curve (25–27). In view of this finding, we characterized ACh concentration responses for mutant (α4)3(β2)2 nAChRs in the absence and presence of CMPI by recording current responses to increasing concentrations of ACh alone and in the presence of 1 μM CMPI from oocytes expressing WT and mutant (α4)3(β2)2 nAChRs (Fig. 6). The ACh concentration-response curve for WT (α4)3(β2)2 nAChR was characterized by an EC_{50} of 99 ± 23 μM (Table 3). Co-application of 1 μM CMPI produced a left shift of the ACh concentration-response curve, decreasing the ACh EC_{50} to 0.6 ± 0.2 μM with little effect, if any, on the ACh maximum response (I_{max} = 98 ± 4%). With the exception of the substitutions α4K64T, α4T126L, and α4T126I, the ACh concentration-response curves for mutant (α4)3(β2)2 nAChRs in the absence of CMPI were characterized by EC_{50} values that were equal or slightly higher than that for WT (Table 3). Co-application of 1 μM CMPI with ACh to oocytes expressing (α4)3(β2)2 nAChRs containing amino acid substitutions at positions α4Leu-37, α4Arg-39, α4His-68, α4His-116, or α4Arg-122 produced a left shift of the ACh concentration-response curve significantly decreasing the ACh EC_{50} (*t* test, $p < 0.01$). For oocytes expressing (α4)3(β2)2

Table 2

CMPI modulation of WT and mutants (α4)3(β2)2 nAChRs

Current responses to 10 μM ACh alone or in the presence of increasing concentrations of CMPI were recorded from oocytes expressing WT and mutants (α4)3(β2)2 nAChRs. For each application peak current amplitude was quantified and normalized to peak current amplitude elicited by 10 μM ACh alone within the same recording run. Replicas from the same oocyte were averaged and for each CMPI concentration (average (Avg) ± S.E.) of data from several oocytes (N) were plotted (Fig. 5) and fit to Equation 1. The probability (*P*) that an I_{max} differs from no potentiation (I_{max} = 100) was analyzed using a one-way analysis of variance with the Holm-Sidak test. Curve-fitting, parameters calculation, and statistics were performed in SigmaPlot 11 (Systat Software Inc.).

	CMPI Potentiation of 10 μM ACh			
Subunits	EC_{50} Ave ± S.E.	I_{max} Ave ± S.E	*N*	*P*
α4:β2	0.18 ± 0.03	386 ± 15	6	<0.001
α4L37I:β2	0.28 ± 0.05	498 ± 31	4	<0.001
α4L37T:β2	0.20 ± 0.04	355 ± 19	5	<0.001
α4R39Q:β2	0.12 ± 0.02	361 ± 11	4	<0.001
α4R39H:β2	0.20 ± 0.04	434 ± 22	4	<0.001
α4G41M:β2	ND	136 ± 7[a]	3	0.195
α4G41E:β2	ND	153 ± 34[a]	5	0.026
α4K64T:β2	ND	140 ± 6[a]	4	0.116
α4E66I:β2	ND	101 ± 3[a]	4	0.968
α4H68N:β2	0.04 ± 0.01	405 ± 12	3	<0.001
α4H68E:β2	0.10 ± 0.01	354 ± 11	3	<0.001
α4H116V:β2	0.13 ± 0.02	542 ± 17	4	<0.001
α4H116L:β2	0.35 ± 0.07	283 ± 16	4	<0.001
α4H116A:β2	0.29 ± 0.06	786 ± 56	3	<0.001
α4R122S:β2	0.17 ± 0.03	342 ± 14	4	<0.001
α4R122E: β2	0.31 ± 0.06	349 ± 15	4	<0.001
α4Q124T:β2	ND	173 ± 14[a]	3	0.010
α4Q124F:β2	ND	140 ± 11[a]	7	0.069
α4T126L:β2	ND	162 ± 6[a]	4	0.016
α4T126I:β2	ND	105 ± 2[a]	6	0.819

[a] Values (average ± S.E.) represent the maximum I_{max} seen for that mutant at any CMPI concentration tested (0.01–3 μM) and not derived from curve-fitting.

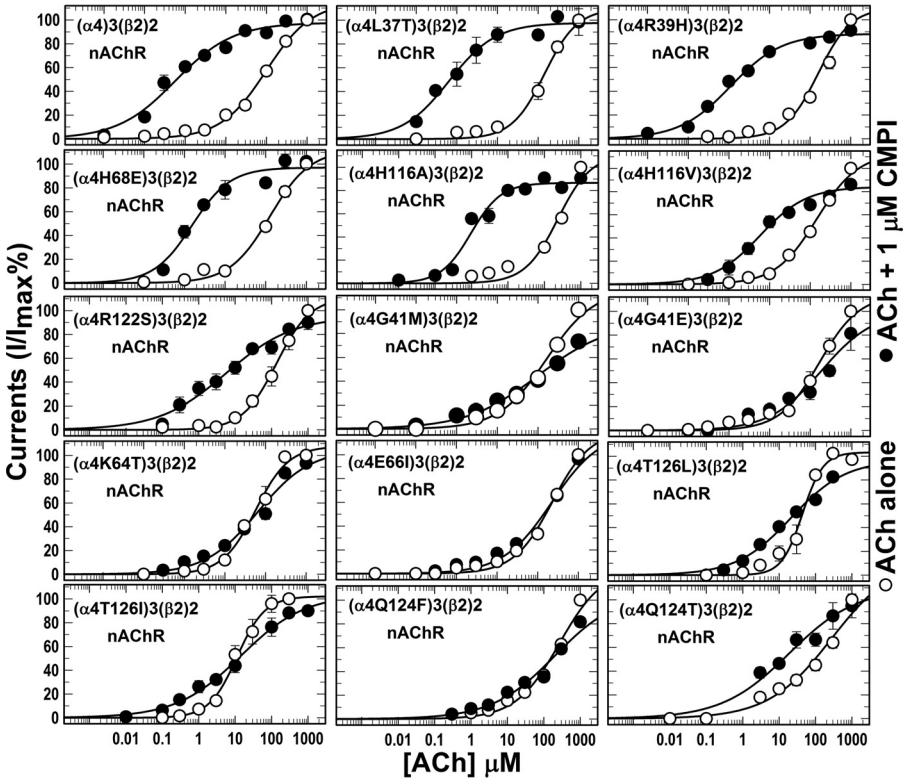

Figure 6. Effect of CMPI on the ACh dose-response curve of WT and mutant (α4)3(β2)2 nAChRs. Currents elicited by *Xenopus* oocytes expressing WT and mutant (α4)3(β2)2 nAChRs in response to 10-s applications of increasing concentrations of ACh (alone (○) or +1 μM CMPI (●)) were recorded and normalized to peak currents elicited by 1 mM ACh alone. Replicas from the same oocyte were averaged, and the average ± S.E. of data from several oocytes were plotted and fit to a single-site model using Equation 1. Parameters (ACh EC_{50} in the presence and absence of CMPI) are shown in Table 3.

nAChRs containing amino acid substitutions at positions α4Gly-41, α4Lys-64, and α4Glu-66, CMPI did not significantly alter the ACh concentration-response curve when co-applied with ACh, and ACh EC_{50} in the presence of 1 μM CMPI and was not significantly different from that in the absence of CMPI. For (α4T126L)3(β2)2 and (α4T126I)3(β2)2 nAChRs, co-application of 1 μM CMPI slightly potentiated current responses at low ACh concentrations (<10 μM) and slightly decreased current responses at higher ACh concentrations, producing a less steep ACh concentration-response curve but with no significant decrease in the ACh EC_{50}. For (α4Q124F)3(β2)2 and (α4Q124T)3(β2)2 nAChRs, the poorly defined maximum response resulted in a large degree of

Table 3

The effect of CMPI on ACh dose-response curve of (α4)3(β2)2 nAChRs

Current responses to increasing concentrations of ACh (alone and in the presence of 1 μM CMPI) were recorded from oocytes expressing WT and mutants (α4)3(β2)2 nAChRs. For each application, peak current amplitude was quantified and normalized to peak current amplitude elicited by 1 mM ACh alone within the same recording run. Replicas from individual oocytes were averaged. For each drug application (average ± S.E.), data from several oocytes (*N*) were plotted (Fig. 6) and fit to Equation 1. The probability (*P*) that the ACh EC_{50} in the presence of CMPI differs from ACh EC_{50} in the absence of CMPI was analyzed by *t* test. Curve-fitting and parameter calculation was performed in SigmaPlot 11 (Systat Software Inc.). One-way analysis of variance of ACh EC_{50} values for WT and mutant (α4)3(β2)2 nAChRs in the absence of CMPI revealed no statistically significant difference ($p = 0.079$). Pairwise *t* test of ACh EC_{50} of (α4K64T)3(β2)2, (α4T126L)3(β2)2, or (α4T126I)3(β2)2 *versus* WT (α4)3(β2)2 nAChR revealed *p* values of 0.39, 0.06, and 0.01, respectively.

	ACh				ACh (+1 μM CMPI)				
Combination	EC_{50}	I_{max} %	h_n	N	EC_{50}	I_{max} %	h_n	*N*	*P*
	μM				μM				
α4:β2	99 ± 23	115 ± 8	0.8 ± 0.1	12	0.6 ± 0.2	98 ± 4	0.6 ± 0.1	6	0.009
α4L37I:β2	250 ± 43	113 ± 6	1.1 ± 0.2	6	0.6 ± 0.1	90.3 ± 3	0.6 ± 0.1	4	0.002
α4L37T:β2	144 ± 20	110 ± 5	1.1 ± 0.2	3	0.6 ± 0.2	98 ± 4	0.7 ± 0.1	3	0.002
α4R39Q:β2	100 ± 11	110 ± 3	0.9 ± 0.1	8	3.6 ± 2.3	75 ± 8	0.5 ± 0.1	6	<0.001
α4R39H:β2	159 ± 17	110 ± 3	1.1 ± 0.1	4	1.1 ± 0.2	88 ± 2	0.7 ± 0.1	3	<0.001
α4G41M:β2	165 ± 41	117 ± 7	0.7 ± 0.1	4	104 ± 86	90 ± 16	0.5 ± 0.1	7	0.624
α4G41E:β2	169 ± 34	114 ± 6	0.9 ± 0.1	4	190 ± 110	100 ± 14	0.7 ± 0.2	5	0.875
α4K64T:β2	57 ± 11	108 ± 6	1.1 ± 0.2	3	65 ± 37	105 ± 15	0.7 ± 0.1	4	0.865
α4E66I:β2	227 ± 78	120 ± 15	0.9 ± 0.1	3	222 ± 173	120 ± 28	0.7 ± 0.2	4	0.986
α4H68N:β2	126 ± 20	111 ± 5	1.0 ± 0.1	5	0.7 ± 0.1	91 ± 4	0.7 ± 0.1	6	<0.001
α4H68E:β2	127 ± 21	112 ± 5	0.9 ± 0.1	4	1.5 ± 0.4	97 ± 5	0.9 ± 0.2	4	<0.001
α4H116V:β2	146 ± 18	113 ± 4	0.9 ± 0.1	5	5.9 ± 1.2	84 ± 3	0.8 ± 0.1	4	<0.001
α4H116A:β2	195 ± 65	100 ± 12	1.3 ± 0.5	3	1.0 ± 0.2	87 ± 3	1.0 ± 0.2	5	<0.001
α4R122S:β2	136 ± 15	111 ± 3	0.9 ± 0.1	4	5.8 ± 2	95 ± 5	0.5 ± 0.1	5	<0.001
α4Q124T:β2	284 ± 236	136 ± 23	0.5 ± 0.1	5	19 ± 10	110 ± 9	0.5 ± 0.1	5	0.294
α4Q124F:β2	269 ± 92	127 ± 11	0.7 ± 0.1	5	202 ± 143	107 ± 15	0.5 ± 0.1	4	0.694
α4T126L:β2	44 ± 7	103 ± 6	1.5 ± 0.3	9	22 ± 12	97 ± 13	0.6 ± 0.1	4	0.223
α4T126I:β2	11 ± 1	102 ± 4	1.1 ± 0.1	7	14 ± 5	104 ± 6	0.5 ± 0.1	7	0.567

uncertainty in ACh EC_{50} calculation, and that precluded determination of any significant effect of CMPI on the ACh EC_{50}.

ACh, CMPI, and NS9283 docking at the α4:α4 extracellular interface

Structural studies, homology models based on available X-ray structures of AChBPs and pentameric ligand-gated ion channels, and the recently published X-ray structure of (α4)2(β2)3 nAChR (5) have identified unique features defining agonist binding at the α4:β2 agonist-binding site (for review, see Refs. 12 and 36). The α4:β2 agonist-binding site is delineated by five conserved aromatic amino acid residues forming a binding "pocket" for the trimethylammonium group of ACh: four from the α4 subunit (α4Tyr-100, α4Trp-156, α4Tyr-197, α4Tyr-204) and one from the β2 subunit (β2Trp-57). The β2 subunit provides additional amino acid residues (*e.g.* β2Val-111, β2Phe-119) that are not conserved among nAChR subunits. The non-canonical α4:α4 subunit extracellular interface is structurally distinct from the α4:β2 agonist-binding site and has a distinctive ligand selectivity imposed by amino acid residues in the complementary α4(−) face (27).

In initial computational docking analyses visualizing the binding sites for CMPI and NS9283 (Fig. 7), we used an (α4)3(β2)2 nAChR homology model based on the structure of *Lymnaea* AChBP crystallized in the presence of the agonist carbamylcholine (PDB accession number 1UV6; Ref. 37). Because we sought to perform docking analyses of CMPI and NS9283 in the absence and presence of ACh, we first docked ACh at the α4:α4 extracellular interface (Fig. 7*B*). The most favorable binding mode of ACh has a CDOCKER interaction energy of −31 kcal/mol with the nitrogen of the trimethylammonium group well coordinated by α4Tyr-100, α4Trp-156, α4Tyr-197, and α4Tyr-204 of the α4(+) face and α4Trp-62 of the α4(-) face. The carbonyl group of the ACh is oriented toward the α4(−) face of the second α4 subunit, within 4.5 Å of α4His-116 (equivalent to β2Val-111, the main amino acid residue in the β2 subunit photolabeled by the agonist [^{3}H]epibatidine (38)), α4Gln-124, and α4Thr-126, and >7 Å from any other non-conserved residue in the α4(−) face.

In the absence of ACh, CMPI docked at the α4:α4 subunit extracellular interface in one most favorable binding mode (Fig. 7*C*) with CDOCKER interaction energy of −36.8 kcal/mol. In this orientation, the piperidine ring of the CMPI occupies the same location as the carbonyl group of ACh, with the CMPI long axis (length, 12.9 Å) extending outward between Segment C of the α4(+) face and beta strands β6 (α4Gln-124/α4Thr-126), β2 (α4Trp-62/α4Lys-64), and β1 (α4Gly-41/α4Ser-43) of the adjacent α4(−) face. In contrast to CMPI, NS9283 in the absence of ACh docked with two equally favorable binding modes (Fig. 7*D*) with CDOCKER interaction energies of −29.1 and −28.8 kcal/mol. In the first binding mode, NS9283 docked deep in the aromatic box with its long axis (length, 12.2 Å) extending upward adjacent to beta strands β5 and β6 of the α4(−) face. In the second binding mode, NS9283 maintained the same long axis orientation but was translocated 3Å closer to the α4(−) face. In both orientations, one end of NS9283 is within 4.0 Å of α4His-114, α4Gln-124, and α4Thr-126 of the α4(−) face.

When CMPI or NS9283 was docked at the α4:α4 subunit extracellular interface in the presence of ACh (Fig. 7, *E* and *F*), the lowest energy solutions for CMPI (−33.3 kcal/mol) and NS9283 (−29.7 kcal/mol) were superimposed along their long axes, with the benzonitrile of NS9283 and piperidine of CMPI within 4 Å of α4His-116. CMPI and NS9283 extend outward at the level of α4Gln-124 (6.6 and 3.1 Å, respectively) and αGlu-66 (11.5 and 5.2 Å, respectively).

In the course of writing this manuscript, the X-ray structure of the agonist-bound (α4)2(β2)3 nAChR was published (5).

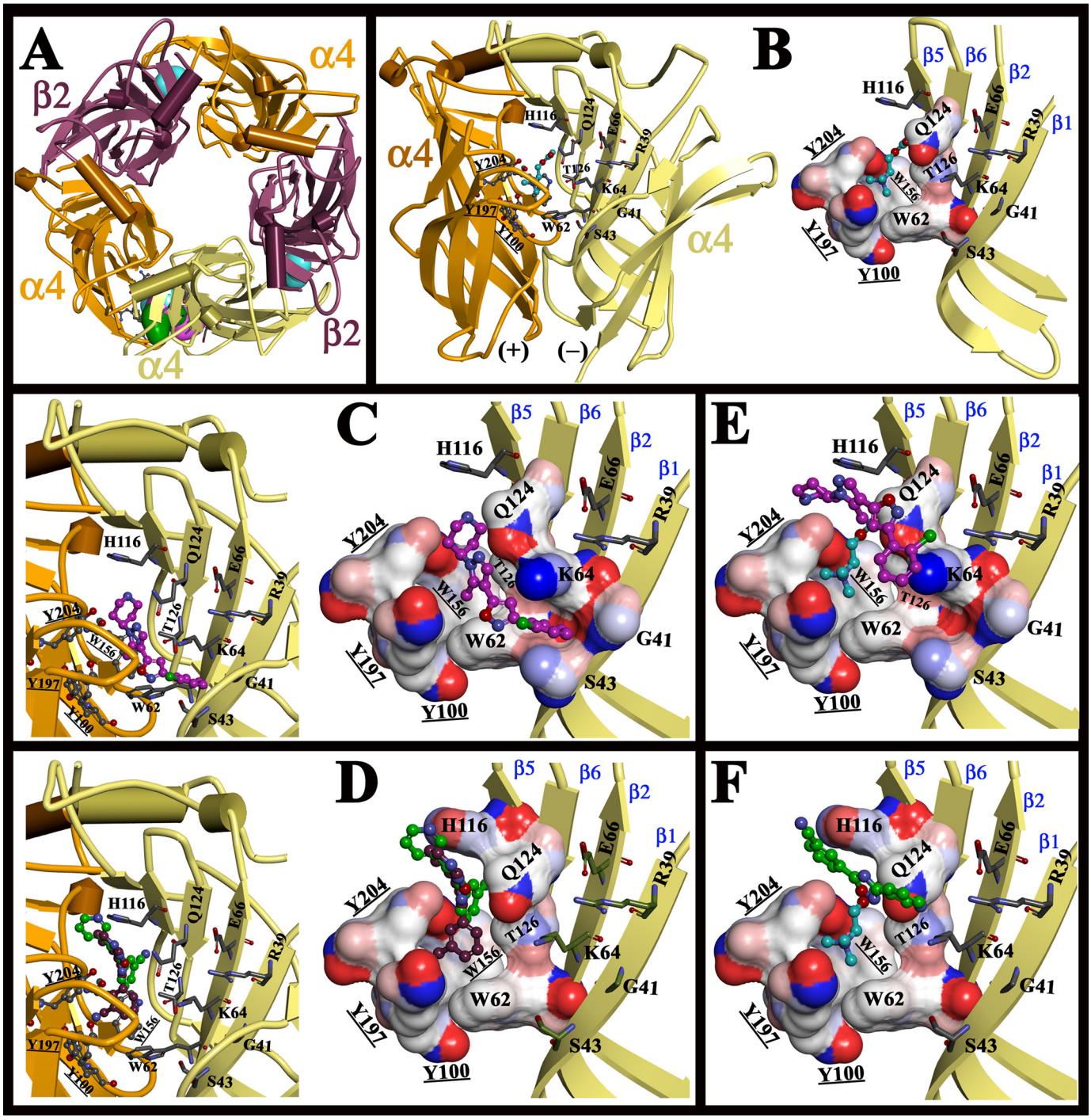

Figure 7. PAM-binding sites at the α4:α4 extracellular interface in a model based on the X-ray structure of agonist-bound AChBP. Top (*A*) and side (*B–F*) views show ACh (*cyan*), CMPI (*magenta*), and NS9283 (*green*) docked at the α4:α4 extracellular interface of an (α4)3(β2)2 nAChR homology model based on the structure of *Lymnaea* AChBP crystallized in the presence of carbamylcholine (PDB accession number 1UV6). Secondary structure of α4 (*brown* and *yellow*) and β2 (*cherry red*) subunits is shown with α-helices as *cylinders* and β-strands as *ribbons* (β1, β2, β5, and β6 are labeled in *blue*). *A*, Connolly surfaces are included for ACh and a superimposition of ACh/CMPI/NS9283 docked at the α4:β2 and α4:α4 extracellular interfaces, respectively. ACh, CMPI, and NS9283 were individually docked to the α4:α4 interface alone (*B–D*), and CMPI and NS9283 were docked in the presence of ACh (*E* and *F*). The lowest energy docking solutions for each ligand are shown in *stick and ball representation*, and amino acid side-chains are shown in *stick representation colored by atom type* (C, *gray*; O, *red*; N, *blue*). For each ligand, conserved amino acid residues that make up the agonist site aromatic box and amino acid residues that significantly reduced its effects when substituted to the corresponding residue from the β2 subunit are shown in Connolly surface representation colored by atom charge (positive, *blue*; negative, *red*). Residues are labeled using the single letter code with those from the α4 (+) face *underlined*.

This structure contains only two α4 subunits and lacks the α4:α4 subunit extracellular interface, the structural domain harboring the CMPI and NS9283 binding sites. We generated an (α4)3(β2)2 nAChR homology model using protein superimposition, as described under "Experimental Procedures," then we performed computational docking analyses for CMPI and NS9283 in the absence of ACh (Fig. 8). CMPI docking at the α4:α4 subunit extracellular interface revealed two favorable

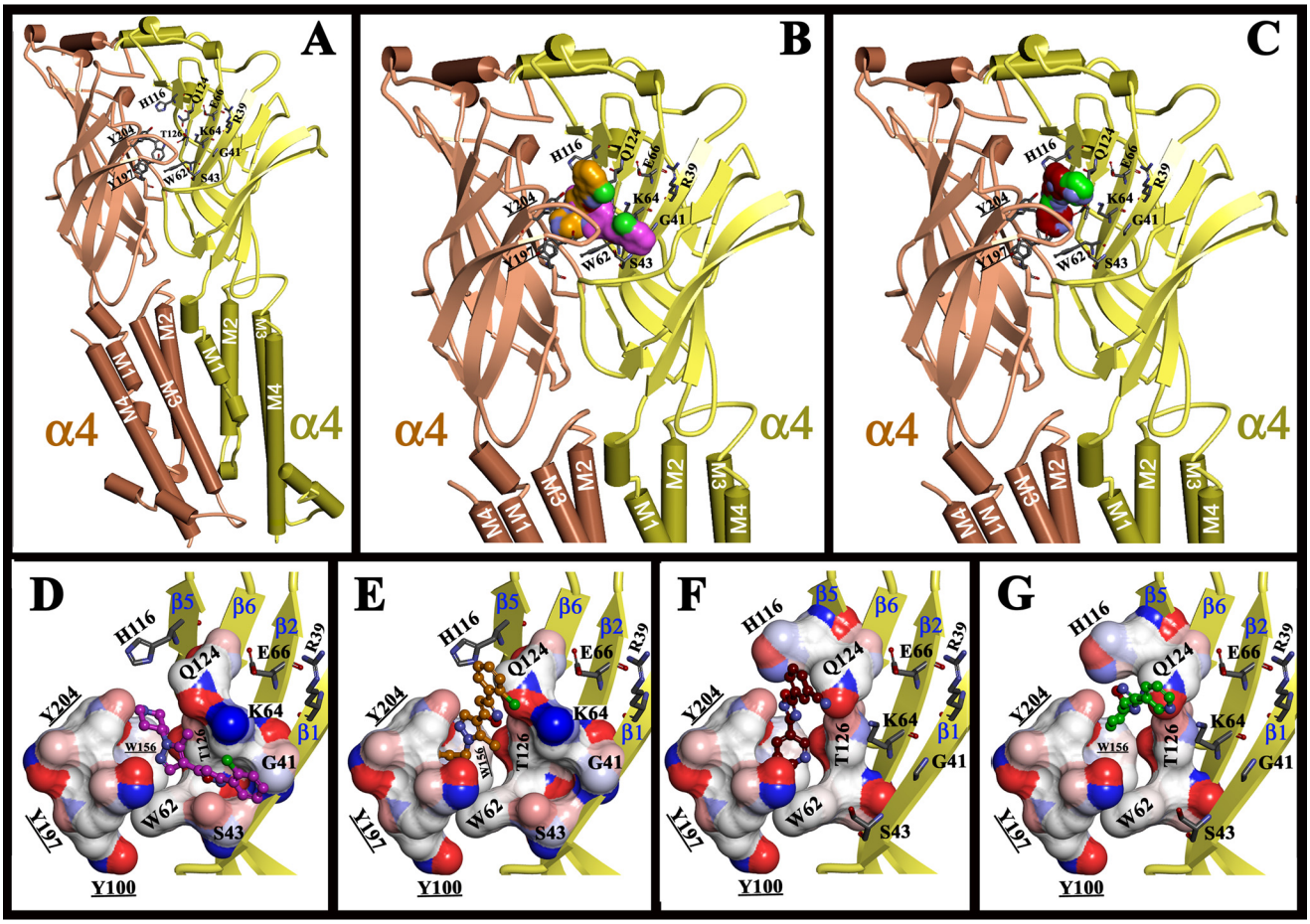

Figure 8. PAM-binding sites at the α4:α4 extracellular interface in a model based on the X-ray structure of agonist-bound (α4)2(β2)3 nAChR. Side views showing CMPI (*magenta* and *brown*) and NS9283 (*green* and *cherry red*) docked at the α4:α4 extracellular interface of (α4)3(β2)2 nAChR homology model based on the X-ray structure of (α4)2(β2)3 nAChR (PDB accession number 5KXI). This model was generated by replacing a β2 subunit with an α4 subunit from the same crystal structure as described under "Experimental Procedures." *A–C*, side views showing secondary structure of two α4 subunits (*brown* and *yellow*) with α-helices as *cylinders* and β-strands as *ribbons*. Amino acid residues contributing to the α4:α4 extracellular interface are shown in *stick representation colored by atom type* (C, *gray*; O, *red*; N, *blue*), and the four transmembrane helices of each α4 subunit are labeled *M1–M4*. Connolly surfaces of a superimposition of the two lowest energy docking solutions for CMPI and NS9283 are shown in *B* and *C*, respectively. *D–G*, close-up side views of the α4:α4 extracellular interface showing the lowest energy docking solutions for CMPI (*D* and *E*) and NS9283 (*F* and *G*) are in *stick and ball representation*. For each ligand, conserved amino acid residues that make up the agonist site aromatic box and amino acid residues that significantly reduced its effects when substituted to the corresponding residue from the β2 subunit are shown in Connolly surface representation colored by atom charge (positive, *blue*; negative, *red*). Residues are labeled using the single letter code with those from the α4 (+) face *underlined*.

binding modes (Fig. 8, *D* and *E*) with CDOCKER interaction energies of −32.3 and −28.3 kcal/mol, respectively. The first CMPI orientation (Fig. 8*D*) resembles the CMPI docking mode obtained using (α4)2(β2)3 nAChR model based on the AChBP structure (Fig. 7*C*). In the second orientation, the piperidine ring of the CMPI docked deeper in the aromatic pocket, with the long axis extending toward the α4(−) face and CMPI maintaining close proximity (<5.0 Å) to α4Gln-124/α4Thr-126/α4Trp-62/α4Lys-64. For NS9283, two docking modes with similar CDOCKER interaction energies of (−26.99 and −26.87 kcal/mol) were predicted (Fig. 8, *F* and *G*). In the first docking mode (Fig. 8*F*) NS9283 shares the long axis location and proximity to α4His-116 (4.1 Å) as seen using obtained using the (α4)2(β2)3 nAChR model based on the AChBP structure (Fig. 7*D*). However, in the second docking mode (Fig. 8*G*), the NS9283 long axis was tilted outward toward α4Gln-124 and α4Thr-126.

In view of the limitations associated with the prediction of binding modes by computational docking using homology models, it was unexpected that calculations based upon the AChBP and (α4)2(β2)3 nAChR structures would result in similar predictions concerning the location of bound CPMI and NS9283. However, both docking analyses predicted close proximity and interactions between CMPI or NS9283 and the amino acid residues that we identified using mutational analyses as molecular determinants for CMPI or NS9283 potentiation of the (α4)3(β2)2 nAChR. Furthermore, CMPI docking at the α4:α4 subunit extracellular interface in the absence and presence of ACh predicted higher affinity in the absence than the presence of ACh, and the binding mode in the absence of ACh was more consistent with the effects of amino acid substitutions on CMPI potentiation of (α4)3(β2)2 nAChR.

Discussion

Overlapping ACh- and PAM-binding sites at the α4:α4 subunit extracellular interface

In this work we used mutational analyses and two-electrode voltage-clamp recording of ACh-induced current from *Xeno-*

pus oocytes to identify a binding site for CMPI, a PAM that is selective for the (α4)3(β2)2 nAChR. The stoichiometry-dependent effects of CMPI (low-sensitivity (α4)3(β2)2 *versus* high-sensitivity (α4)2(β2)3 nAChR) and its inability to potentiate α3β2 nAChR predicted a CMPI recognition site(s) at the α4:α4 subunit interface that is present only in the (α4)3(β2)2 nAChR isoform. Because the (−) face of the α4 subunit is what makes the α4:α4 subunit interface different from other subunit interfaces, we examined the effects of amino acid substitutions at the α4 subunit (−) face that project toward the α4:α4 subunit interface on (α4)3(β2)2 nAChR potentiation by CMPI, NS9283 (another PAM with (α4)3(β2)2 nAChR isoform selectivity), and dFBr ((α4)3(β2)2/(α4)2(β2)3 nAChRs PAM).

A total of 15 amino acid positions, 10 within the extracellular domain and 5 within the transmembrane domain, were substituted individually to their corresponding amino acid residues in the α3 and/or β2 nAChR subunits. Within these substitutions, one position (His-116) selectively reduced potentiation by NS9283, whereas three positions (Gly-41, Lys-64, and Glu-66) selectively reduced potentiation by CMPI. Substitutions at two positions (Gln-124 and Thr-126) reduced potentiation by CMPI and NS9283. Amino acid substitution at the other nine positions did not significantly reduce potentiation by CMPI or NS9283, and none of the substitutions reported here had a significant effect on (α4)3(β2)2 nAChR potentiation by dFBr.

To gain further insight into the binding modes of CMPI/NS9283, we performed computational analyses docking CMPI and NS9283 at the α4:α4 subunit extracellular interface in the absence and presence of ACh bound at this interface. Our computational analyses (summarized in Fig. 7 and Fig. 8) predicted stable binding of CMPI and NS9283 at the α4:α4 interface in the absence or presence of ACh but with different amino acid residue contacts. The functional consequences of amino acid substitutions and the predicted interactions of docked CMPI/NS9283 with these amino acid residues establish that NS9283/CMPI potentiate (α4)3(β2)2 nAChR by replacing ACh at the α4:α4 subunit interface by binding to pockets that completely (NS9283) or partially (CMPI) overlap the ACh-binding site.

PAM recognition at the α4:α4 extracellular interface

CMPI recognition at the α4:α4 subunit extracellular interface differs from that for NS9283 and for agonists that bind at the α4:α4 subunit extracellular interface, especially in regard to the role of amino acid residues in the complementary α4(−) face. Amino acid substitutions at positions α4Gly-41 and α4Lys-64 to the corresponding amino acid residues in the β2 subunit (methionine and threonine, respectively) selectively reduced potentiation by CMPI but not NS9283 or dFBr. In agreement with these findings, our computational analyses in the absence of ACh predicted CMPI binding in close proximity to α4Gly-41 and α4Lys-64 with the latter predicted to form hydrophobic interactions with the chlorobenzene and isoxazole of CMPI. This hydrophobic interaction between α4Lys-64 and the chlorobenzene ring appears essential for CMPI potentiation, as replacement of the chlorobenzene ring by non-substituted benzene or cyclohexane increased CMPI EC_{50} by ~60- and ~250-fold, respectively (31).

In contrast, amino acid substitutions at α4His-116 did not reduce CMPI potentiation of (α4)3(β2)2 nAChR, and there is no predicted interaction between α4His-116 and docked CMPI in the absence of ACh. α4His-116 is considered the main molecular determinant for (α4)3(β2)2 nAChR potentiation by NS9283 (17). Indeed, amino acid substitutions at α4His-116, α4Gln-124, and α4Thr-126, but not any other non-conserved position within the α4(−) face (Fig. 4 and Table 1), significantly reduced NS9283 potentiation of (α4)3(β2)2 nAChR, and NS9283 docked in close proximity to these amino acid residues. These results emphasize the role of β strands 5 and 6 of the complementary α4(−) face in NS9283 binding. They contribute mainly polar amino acid residues (His/Thr/Gln), whereas β strands 5 and 6 of the complementary β2(−) face of the α4:β2 extracellular interfaces contribute mainly hydrophobic amino acid residues (Val/Phe/Leu). Furthermore, the presence of histidine at this position in the α4:α4 subunit extracellular interface has been shown to impose a "steric limit" on the size of agonist (length <7 Å) that can bind at the α4:α4 subunit extracellular interface (27). This steric limit did not hinder the ability of CMPI (length 12.9 Å) to enter and bind at the α4:α4 subunit extracellular interface. A simple interpretation would be that, unlike NS9283 and other agonists, CMPI occupies a binding site shifted away from α4His-114 and in proximity to α4Gly-41/α4Ser43, consistent with the fact that substitutions at α4Gly-41 to larger amino acids residue (glutamate or methionine) reduced CMPI potentiation.

In addition to CMPI interactions with non-conserved amino acid residues of the α4(−) face, CMPI in its most favorable binding mode in the absence of ACh interacts with conserved core aromatics of the α4(-) and α4(+) faces. The CMPI piperidine ring, which is a strong base and can be protonated, occupies the same position as the carbonyl group of ACh and is in close proximity to (and predicted to form H-bonds) with both the carbonyl group of α4Trp-154 and the hydroxyl group of α4Tyr-204. The methyl substitution at the pyrazole ring is predicted to form π-alkyl bonds, two with the benzene and pyrrole rings of α4Trp-156 (α4 (+) face) and one with the benzene of α4Trp-62 (α4(−) face). Indeed, the methyl substitution enhanced the potency of CMPI by ~7-fold over non-substituted pyrazole (H instead of CH_3), and replacement of the methyl by an ethyl group further enhanced CMPI potency as an α4β2 nAChR potentiator (31). We predict that longer alkyl substituents would further enhance the hydrophobic interaction of CMPI with these core aromatic residues in the α4:α4 subunit interface.

Relevance to allosteric modulation of nAChR

In contrast to the canonical α4:β2 agonist-binding sites, the structural features, ligand-binding, and functional contributions of the non-canonical α4:α4 agonist-binding site are still under ongoing investigation. Nevertheless, published studies of the pharmacology of high and low sensitivity α4β2 nAChRs have established that the α4:α4 agonist-binding site is structurally and functionally distinct from the α4:β2 agonist-binding sites and that the α4:β2 agonist-binding sites of the (α4)3(β2)2 and (α4)2(β2)3 nAChR are functionally non-equivalent (17, 25–27). ACh binds to the α4:β2 agonist-binding sites of

(α4)2(β2)3 and (α4)3(β2)2 nAChRs with similar apparent affinity (EC_{50} ~1 μM). However, ACh occupancy of the two α4:β2 agonist-binding sites of the (α4)2(β2)3 but not the (α4)3(β2)2 nAChR is sufficient for full receptor activation. In the (α4)3(β2)2 nAChR, full ACh occupancy of the two α4:β2 agonist-binding sites results in only ~20% of full activation with full activation achieved at higher ACh concentrations (EC_{50} ~100 μM) when the α4:α4 agonist-binding site is occupied. Using this mechanistic model, the effect of CMPI on ACh-induced responses of (α4)3(β2)2 nAChR activation can be viewed as a co-agonistic or allosteric effect. In both cases, CMPI occupies the α4:α4 extracellular interface with much higher affinity than ACh and renders the α4:β2 agonist-binding sites of the (α4)3(β2)2 nAChR functionally equivalent to the α4:β2 agonist-binding sites of the (α4)2(β2)3 nAChR (*i.e.* ACh binding at the α4:β2 agonist-binding sites results in full activation of (α4)3(β2)2 nAChR). At macroscopic current levels, CMPI potentiation of (α4)3(β2)2 nAChR was characterized by an increase of ACh potency with no effect on the maximum ACh-induced current (Fig. 6). This pharmacological profile supports an allosteric mechanism for CMPI potentiation. Nevertheless, further studies using patch-clamp and single-channel recording are required to further clarify the mechanism of CMPI potentiation of (α4)3(β2)2 nAChR.

Despite binding with high affinities at the α4:α4 interface, CMPI and NS9283 lack agonist activity in wild-type (α4)3(β2)2 nAChRs. Their binding at the α4:α4 extracellular interface potentiates current responses triggered by ACh binding at the α4:β2 agonist-binding sites. The higher affinity of CMPI and NS9283 for the α4:α4 *versus* α4:β2 interface could explain their lack of agonist activity, as binding of at least two agonist molecules is required for channel gating (25). Indeed, NS9283 acted as an agonist in (α4)3(β2)2 nAChRs mutated to contain two α4:α4-like agonist-binding sites (17). Although more studies are needed to fully understand the pharmacology of the α4:α4 drug-binding sites, the work presented here provides comprehensive analyses of the role of the α4:α4 extracellular interface in the allosteric modulation of α4β2 nAChRs. The results of this study will facilitate the design and development of novel α4β2 nAChR-selective ligands with potential experimental and clinical applications.

Experimental procedures

Materials

CMPI was a generous gift from Drs. Stefan McDonough and Alessandro Boezio (Amgen Inc. Cambridge, MA; Ref. 30). dFBr and NS9283 were from TOCRIS Bioscience R&D (Minneapolis, MN). Collagenase type 2 was from Worthington Biomedical, Lakewood, NJ. Acetylcholine chloride and other chemicals were purchased from Sigma unless otherwise indicated in the text.

cDNA plasmids and site-directed mutagenesis

pSP64 poly(A) plasmids with cDNA encoding for human α4 or β2 nAChR subunit were generously provided by Dr. Jon Lindstrom (University of Pennsylvania). Point mutations were introduced into plasmid expression vectors coding for the α4 nAChR subunit using the QuikChange II Site-Directed Mutagenesis Kit (Agilent Technologies) then confirmed by DNA sequencing (GENEWIZ, LLC., South Plainfield, NJ). For each point mutation within α4, two custom-designed complimentary oligos containing the desired mutation were ordered from Integrated DNA Technologies (Coralville, IA). Amino acid numbers are based on the mature α4 subunit; add 28 to convert to amino acid numbering starting from the transitional N terminus (methionine 1) of the α4 subunit.

Receptor expression in Xenopus oocytes

cDNA plasmids of wild-type (WT) and mutant nAChR subunits were linearized with AseI (*h*α4) and PvuII (*h*β2), then cRNA transcripts suitable for oocytes expression were prepared from linearized plasmid using SP6 mMESSAGE mMACHINE high yield capped RNA transcription kits (Ambion) following the manufacturer's protocol. RNA concentration was estimated from the A_{260} (with 260/280 ratio >1.9) and mixed at ratios 8α:1β or 1α:8β to express nAChRs with subunit stoichiometries of 3α:2β or 2α:3β, respectively. The final concentration of the subunits RNA mixture was adjusted to 100–200 ng/μl with nuclease-free water, and oocytes were injected with a volume containing 5–20 ng of cRNA.

Oocytes-positive female *X. laevis* were purchased from NASCO (Fort Atkinson, WI), and ovarian lobules were harvested surgically following animal use protocols approved by the Texas A&M Health Sciences Center Institutional Animals Care and Use Committee. The lobules were treated with 3 mg/ml collagenase type 2 (Worthington Biomedical) with gentle shaking for 3 h at room temperature in Ca^{+2}-free OR2 buffer (85 mM NaCl, 2.5 mM KCl, 1 mM $MgCl_2$, 5 mM HEPES, pH 7.6). Stage V and VI oocytes were selected, injected with cRNA, and incubated at 18 °C in ND96-gentamicin buffer (96 mM NaCl, 2 mM KCl, 1.8 mM $CaCl_2$, 1 mM $MgCl_2$, 5 mM HEPES, 50 μg/ml gentamicin, pH 7.6) for 24–72 h to allow receptor expression.

Electrophysiological recording

A standard two-electrode voltage-clamp technique was used as described previously (30, 33) to acquire whole cell current from oocytes expressing WT or a mutant nAChR in response to drug(s) application. *Xenopus* oocytes were voltage-clamped at −50 mV using Oocyte Clamp OC-725C (Warner Instruments) in a custom-made small recording chamber and under continuous perfusion with recording buffer (100 mM NaCl, 2 mM KCl, 1 mM $CaCl_2$, 0.8 mM $MgCl_2$, 1 mM EGTA, 10 mM HEPES, pH 7.5). An automated perfusion system made up of glass reservoirs and Teflon tubing (Warner Instruments) was used to control recording chamber perfusion and drug application. Each recording run included 3–6 drug applications (10 s each) separated by 90-s wash intervals unless otherwise specified in the figure legends, and oocytes were washed for 3–5 min between runs. Each drug concentration was tested at least two times per oocyte and repeated on a number of oocytes (*N*) as specified in Tables 1–3. Current traces were digitized at 50 Hz and analyzed, and peak current amplitudes in response to drug applications were quantified using Digidata 1550A interface/pCLAMP 10.4 software (Molecular Devices). CMPI and NS9283 were prepared as 10 mM stock solution in DMSO, and

dFBr was prepared as 5 mM stock solution in water. Stock solutions were stored at −20 °C and diluted to final concentrations in recording buffer on the day of experiments. At the highest concentration tested, DMSO was present at 0.1%, which had no effect on ACh responses.

Data analysis

Data analyses, parameter calculations, and statistical analyses were performed using Excel (Microsoft Corp.) and Sigmaplot v11 (Systat Software Inc.). For concentration-dependent potentiation of ACh-induced currents by CMPI, peak current amplitudes in response to co-applications of CMPI with 10 μM ACh were normalized to the peak current amplitude elicited by 10 μM ACh alone within same recording run. For ACh concentration-response curves in the absence or presence of CMPI, peak current amplitudes in response to co-applications of increasing concentrations of ACh (±1 μM CMPI) were normalized to the peak current amplitude elicited by 1 mM ACh alone within same recording run. Replicas from the same oocyte were combined (average ± S.D.; the oocyte with S.D. of >30% of its average was rejected), and data (average ± S.E.) from *N* oocytes were plotted and fit to a 3-parameter Hill equation,

$$Ix = I_0 + I_{max}/(1 + (EC_{50}/x)^h) \quad \text{(Eq. 1)}$$

where *Ix* is the normalized ACh current in the presence of CMPI at concentration x, I_{max} is the maximum potentiation of current, *h* is the Hill coefficient, and EC_{50} is the CMPI concentration producing 50% of maximal potentiation. For CMPI enhancement, $I_0 = 100$, and the probability (*P*) that the I_{max} differs from no potentiation ($I_{max} = 100$) was analyzed using one-way analysis of variance with the Holm-Sidak test and is reported in Table 2. For ACh concentration response, $I_0 = 0$, and the probability (*P*) that the ACh EC_{50} in the presence of CMPI differs from ACh EC_{50} in the absence of CMPI was analyzed by the *t* test and is reported in Table 3.

Molecular modeling

Homology modeling and docking simulations (CDOCKER) were performed using the Discovery Studio 2017 molecular modeling package from Accelrys. Homology models based on two different X-ray crystallographic structures were constructed as follows.

A homology model of the extracellular domain of the human (α4)3(β2)2 nAChR was constructed from the structure of the *Lymnaea stagnalis* AChBP crystallized with carbamylcholine (PDB accession number 1UV6; Ref. 37) by replacing subunits A, C, and E with α4 residues and B and D with β2 residues. The computer-generated alignment was checked to ensure insertions/deletions occurred outside secondary structure motifs (α-helices or β-sheets). The alignment between α4 and AChBP began with α4His-9 (amino acid numbering is for mature protein according to the X-ray structure of human (α4)2(β2)3 nAChRs (PDB accession number 5KXI; add 26 to obtain amino acid numbers starting from the translational N terminus) and with AChBP L1 and required α4 insertions of residues Asn-31, Asp-78, Tyr-79, Gly-105, and Phe-144 and an AChBP deletion at residue Tyr-168. The alignment between β2 and AChBP began with β2 Asp-2 (amino acid numbering is for mature protein; add 25 to obtain amino acid numbers starting from the translational N terminus) and with AChBP L1 and required β2 insertions of residues Lys-19, Lys-20, Gly-27, Phe-74, Asp-75, Asp-99, and Phe-13 and AChBP deletions of residues Ser-162, Ser-186, Cys-187, and Cys-188. Carbamylcholine molecules were placed into the two α4:β2 agonist sites and the α4:α4 interface site in orientations approximating that of carbamylcholine in the crystal structure, and the model was minimized to -2.30×10^4 kcal/mol. The carbamylcholine molecule was removed from the α4-α4 interface site before docking.

Additional docking on the 1UV6.PDB-based model was performed after first identifying (by docking) the preferred binding site for acetylcholine, placing an acetylcholine molecule in the α4:α4 binding site, and minimizing (−22,937 kcal/mol final energy). A 12 Å binding-site sphere was used with its center between α4Gln-122 and α4Cys-198, and eight randomly positioned CMPI and NS9283 molecules were docked within this binding-site sphere using the same parameters described above.

A homology model of (α4)3(β2)2 nAChR was constructed from the human (α4)2(β2)3 nAChR crystal structure (PDB accession number 5KXI; Ref. 3) by using the "Superimpose Proteins" tool to superimpose a copy of the α4 subunit, designated A, onto the β2 subunit, designated B. This was necessary as the 5KXI.PDB structure does not contain an α4-α4 interface which is the focus of this work. The superimposition was accomplished by minimizing the distances between pairs of tethered α-carbons of 4 conserved residues: β2Pro-219 tethered with α4Pro-227 (M1); β2Trp-57 with α4Trp-62 (aromatic box); β2Cys-130 with α4Cys-135 (Cys-loop); β2Gly-116 with α4Gly-121 (agonist site loop E). Once the copied α4 was superimposed over the β2-B subunit's position, the β2-B subunit was deleted, and the new α4-B was inserted into the structure. This method was used in an attempt to preserve as much as possible the crystal structure of the α4β2 nAChR. The nicotine molecule originally between subunits A (α4) and B (β2) was left in place in the homology model now at the α4-α4 interface, and minimal energy minimization (5 cycles) was performed to reduce any strain interactions due to the subunit replacement (initial energy, 1.78×10^{10} kcal/mol; final energy, -8.39×10^4 kcal/mol; for reference, 5KXI.PDB had initial energy of -5.29×10^4 kcal/mol and 10 minimization cycles produced -8.46×10^4 kcal/mol). The nicotine molecule was removed from the α4:α4 interface site before docking. Initial docking studies with CMPI yielded no solutions with favorable interaction energies (lowest energy solutions were ~−1 kcal/mol). To allow CMPI to dock within the α4:α4 binding site, side chains of Lys-64, Gln-124, and Thr-126 on the minus face were reoriented to mimic the 1UV6.PDB-based homology model that readily docked CMPI.

For docking, eight structurally different molecules of CMPI and NS9283 were seeded together in random orientations and used to dock to the α4:α4 interface "agonist" sites for each model using CDOCKER. CDOCKER is a CHARMm-based molecular dynamics simulated annealing program that treats the ligand as fully flexible while maintaining a rigid receptor (39, 40). A binding-site sphere of radius 12 Å was used that was centered on the location of carbamylcholine or nicotine in the respective models. We configured the docking parameters so

that each of the 8 seeded ligands was subjected to 40+ high-temperature molecular dynamic-induced structural alterations and 40+ random translation/rotation reorientations, producing a total of 1600+ attempts at docking. For each attempt, the ligand and the amino acids within the binding sphere were subjected to simulated annealing, and a full potential final minimization step from which the ligand-receptor interaction energies was calculated. The orientation of the ligand and the calculated interaction energies were collected for the 50 lowest energy solutions for each seeded ligand.

Author contributions—A. K. H. designed and supervised the research and wrote the paper. Z.-J. W., F. D., T. S. M., and K. R. performed the research and the analyzed data. D. C. C. performed the molecular modeling. All authors contributed to reading and editing the manuscript.

Acknowledgment—We thank Dr. Jonathan B. Cohen (Dept. of Neurobiology, Harvard Medical School) for indispensable advice and comments during the course of this study.

References

1. Taly, A., Corringer, P.-J., Guedin, D., Lestage, P., and Changeux, J.-P. (2009) Nicotinic receptors: allosteric transitions and therapeutic targets in the nervous system. *Nat. Rev. Drug Discov.* **8,** 733–750
2. Hurst, R., Rollema, H., and Bertrand, D. (2013) Nicotinic acetylcholine receptors: from basic science to therapeutics. *Pharmacol. Ther.* **137,** 22–54
3. Morales-Perez, C. L., Noviello, C. M., and Hibbs, R. E. (2016) X-ray structure of the human α4β2 nicotinic receptor. *Nature* **538,** 411–415
4. Grupe, M., Grunnet, M., Bastlund, J. F., and Jensen, A. A. (2015) Targeting α4β2 nicotinic acetylcholine receptors in central nervous system disorders: perspectives on positive allosteric modulation as a therapeutic approach. *Basic Clin. Pharmacol. Toxicol.* **116,** 187–200
5. Dineley, K. T., Pandya, A. A., and Yakel, J. L. (2015) Nicotinic ACh receptors as therapeutic targets in CNS disorders. *Trends Pharmacol. Sci.* **36,** 96–108
6. Gotti, C., Zoli, M., and Clementi, F. (2006) Brain nicotinic acetylcholine receptors: native subtypes and their relevance. *Trends Pharmacol. Sci.* **27,** 482–491
7. Benwell, M. E., Balfour, D. J., and Anderson, J. M. (1988) Evidence that tobacco smoking increases the density of (−)-[^{3}H]nicotine binding sites in human brain. *J. Neurochem.* **50,** 1243–1247
8. Picciotto, M. R., Zoli, M., Rimondini, R., Léna, C., Marubio, L. M., Pich, E. M., Fuxe, K., and Changeux, J.-P. (1998) Acetylcholine receptors containing the β2 subunit are involved in the reinforcing properties of nicotine. *Nature* **391,** 173–177
9. Zoli, M., Picciotto, M. R., Ferrari, R., Cocchi, D., and Changeux, J.-P. (1999) Increased neurodegeneration during ageing in mice lacking high-affinity nicotine receptors. *EMBO J.* **18,** 1235–1244
10. Wevers, A., Monteggia, L., Nowacki, S., Bloch, W., Schütz, U., Lindstrom, J., Pereira, E. F., Eisenberg, H., Giacobini, E., de Vos, R. A., Steur, E. N., Maelicke, A., Albuquerque, E. X., and Schröder, H. (1999) Expression of nicotinic acetylcholine receptor subunits in the cerebral cortex in Alzheimer's disease: histotopographical correlation with amyloid plaques and hyperphosphorylated-tau protein. *Eur. J. Neurosci.* **11,** 2551–2565
11. Williams, D. K., Wang, J., and Papke, R. L. (2011) Positive allosteric modulators as an approach to nicotinic acetylcholine receptor-targeted therapeutics: advantages and limitations. *Biochem. Pharmacol.* **82,** 915–930
12. Corringer, P.-J., Le Novère, N., and Changeux, J.-P. (2000) Nicotinic receptors at the amino acid level. *Annu. Rev. Pharmacol. Toxicol.* **40,** 431–458
13. Moroni, M., Zwart, R., Sher, E., Cassels, B. K., and Bermudez, I. (2006) α4β2 nicotinic receptors with high and low acetylcholine sensitivity: pharmacology, stoichiometry, and sensitivity to long-term exposure to nicotine. *Mol. Pharmacol.* **70,** 755–768
14. Seo, S., Henry, J. T., Lewis, A. H., Wang, N., and Levandoski, M. M. (2009) The positive allosteric modulator morantel binds at noncanonical subunit interfaces of neuronal nicotinic acetylcholine receptors. *J. Neurosci.* **29,** 8734–8742
15. Hamouda, A. K., Stewart, D. S., Husain, S. S., and Cohen, J. B. (2011) Multiple transmembrane binding Sites for *p*-trifluoromethyldiazirinyl etomidate, a photoreactive *Torpedo* nicotinic acetylcholine receptor allosteric inhibitor. *J. Biol. Chem.* **286,** 20466–20477
16. Hamouda, A. K., Kimm, T., and Cohen, J. B. (2013) Physostigmine and galantamine bind in the present of agonist at the canonical and noncanonical subunit interfaces of nicotinic acetylcholine receptors. *J. Neurosci.* **33,** 485–494
17. Olsen, J. A., Ahring, P. K., Kastrup, J. S., Gajhede, M., and Balle, T. (2014) Structural and functional studies of the modulator ns9283 reveal agonist-like mechanism of action at α4β2 nicotinic acetylcholine receptors. *J. Biol. Chem.* **289,** 24911–24921
18. Young, G. T., Zwart, R., Walker, A. S., Sher, E., and Millar, N. S. (2008) Potentiation of α7 nicotinic acetylcholine receptors via an allosteric transmembrane site. *Proc. Natl. Acad. Sci. U.S.A.* **105,** 14686–14691
19. Nirthanan, S., Garcia, G., 3rd, Chiara, D. C., Husain, S. S., and Cohen, J. B. (2008) Identification of binding sites in the nicotinic acetylcholine receptor for TDBzl-etomidate, a photoreactive positive allosteric effector. *J. Biol. Chem.* **283,** 22051–22062
20. Jin, X., and Steinbach, J. H. (2011) A portable site: a binding element for 17β-estradiol can be placed on any subunit of a nicotinic α4β2 receptor. *J. Neurosci.* **31,** 5045–5054
21. Wang, J., Kuryatov, A., Jin, Z., Norleans, J., Kamenecka, T. M., Kenny, P. J., and Lindstrom, J. (2015) A novel α2/α4 subtype-selective positive allosteric modulator of nicotinic acetylcholine receptors acting from the c-tail of an α subunit. *J. Biol. Chem.* **290,** 28834–28846
22. Uteshev, V. V. (2016) Allosteric modulation of nicotinic acetylcholine receptors: the concept and therapeutic trends. *Curr. Pharm. Des.* **22,** 1986–1997
23. Zwart, R., and Vijverberg, H. P. (1998) Four pharmacologically distinct subtypes of α4β2 nicotinic acetylcholine receptor expressed in *Xenopus laevis* oocytes. *Mol. Pharmacol.* **54,** 1124–1131
24. Nelson, M. E., Kuryatov, A., Choi, C. H., Zhou, Y., and Lindstrom, J. (2003) Alternate stoichiometries of α4β2 nicotinic acetylcholine receptors. *Mol. Pharmacol.* **63,** 332–341
25. Harpsøe, K., Ahring, P. K., Christensen, J. K., Jensen, M. L., Peters, D., and Balle, T. (2011) Unraveling the high- and low-sensitivity agonist responses of nicotinic acetylcholine receptors. *J. Neurosci.* **31,** 10759–10766
26. Eaton, J. B., Lucero, L. M., Stratton, H., Chang, Y., Cooper, J. F., Lindstrom, J. M., Lukas, R. J., and Whiteaker, P. (2014) The unique α4(+)/(−)α4 agonist-binding site in (α4)3(β2)2 subtype nicotinic acetylcholine receptors permits differential agonist desensitization pharmacology versus the (α4)2(β2)3 subtype. *J. Pharmacol. Exp. Ther.* **348,** 46–58
27. Mazzaferro, S., Gasparri, F., New, K., Alcaino, C., Faundez, M., Iturriaga Vasquez, P., Vijayan, R., Biggin, P. C., and Bermudez, I. (2014) Non-equivalent ligand selectivity of agonist sites in (α4β2)2α4 nicotinic acetylcholine receptors: a key determinant of agonist efficacy. *J. Biol. Chem.* **289,** 21795–21806
28. Timmermann, D. B., Sandager-Nielsen, K., Dyhring, T., Smith, M., Jacobsen, A. M., Nielsen, E. Ø., Grunnet, M., Christensen, J. K., Peters, D., Kohlhaas, K., Olsen, G. M., and Ahring, P. K. (2012) Augmentation of cognitive function by NS9283, a stoichiometry-dependent positive allosteric modulator of α2- and α4-containing nicotinic acetylcholine receptors. *Br. J. Pharmacol.* **167,** 164–182
29. Jin, X., Bermudez, I., and Steinbach, J. H. (2014) The nicotinic α5 subunit can replace either an acetylcholine-binding or nonbinding subunit in the α4β2* neuronal nicotinic receptor. *Mol. Pharmacol.* **85,** 11–17
30. Hamouda, A. K., Deba, F., Wang, Z. J., and Cohen, J. B. (2016) Photolabeling a nicotinic acetylcholine receptor (nachr) with an (α4)3(β2)2 nachr-selective positive allosteric modulator. *Mol. Pharmacol.* **89,** 575–584
31. Albrecht, B. K., Berry, V., Boezio, A. A., Cao, L., Clarkin, K., Guo, W., Harmange, J. C., Hierl, M., Huang, L., Janosky, B., Knop, J., Malmberg, A.,

McDermott, J. S., Nguyen, H. Q., Springer, S. K., Waldon, D., Woodin, K., and McDonough, S. I. (2008) Discovery and optimization of substituted piperidines as potent, selective, CNS-penetrant α4β2 nicotinic acetylcholine receptor potentiators. *Bioorg. Med. Chem. Lett.* **18,** 5209–5212

32. Olsen, J. A., Kastrup, J. S., Peters, D., Gajhede, M., Balle, T., and Ahring, P. K. (2013) Two distinct allosteric binding sites at α4β2 nicotinic acetylcholine receptors revealed by NS206 and NS9283 give unique insights to binding activity-associated linkage at Cys-loop receptors. *J. Biol. Chem.* **288,** 35997–36006
33. Hamouda, A. K., Wang, Z. J., Stewart, D. S., Jain, A. D., Glennon, R. A., and Cohen, J. B. (2015) Desformylflustrabromine (dFBr) and [^{3}H]dFBr-labeled binding sites in a nicotinic acetylcholine receptor. *Mol. Pharmacol.* **88,** 1–11
34. Weltzin, M. M., and Schulte, M. K. (2015) Desformylflustrabromine modulates α4β2 neuronal nicotinic acetylcholine receptor high- and low-sensitivity isoforms at allosteric clefts containing the β2 subunit. *J. Pharmacol. Exp. Ther.* **354,** 184–194
35. Sala, F., Mulet, J., Reddy, K. P., Bernal, J. A., Wikman, P., Valor, L. M., Peters, L., König, G. M., Criado, M., and Sala, S. (2005) Potentiation of human α4β2 neuronal nicotinic receptors by a *Flustra foliacea* metabolite. *Neurosci. Lett.* **373,** 144–149
36. Corringer, P.-J., Poitevin, F., Prevost, M. S., Sauguet, L., Delarue, M., and Changeux, J.-P. (2012) Structure and pharmacology of pentameric receptor channels: from bacteria to brain. *Structure* **20,** 941–956
37. Celie, P. H., van Rossum-Fikkert, S. E., van Dijk, W. J., Brejc, K., Smit, A. B., and Sixma, T. K. (2004) Nicotine and carbamylcholine binding to nicotinic acetylcholine receptors as studied in AChBP crystal structures. *Neuron* **41,** 907–914
38. Srivastava, S., Hamouda, A. K., Pandhare, A., Duddempudi, P. K., Sanghvi, M., Cohen, J. B., and Blanton, M. P. (2009) [^{3}H]Epibatidine photolabels non-equivalent amino acids in the agonist-binding sites of torpedo and α4β2 nicotinic acetylcholine receptors. *J. Biol. Chem.* **284,** 24939–24947
39. Brooks, B. R., Bruccoleri, R. E., Olafson, B. D., States, D. J., Swaminathan, S., and Karplus, M. (1983) CHARMM: A program for macromolecular energy, minimization, and dynamics calculations. *J. Comput. Chem.* **4,** 187–217 10.1002/jcc.540040211
40. Wu, G., Robertson, D. H., Brooks, C. L., 3rd, and Vieth, M. (2003) Detailed analysis of grid-based molecular docking: a case study of CDOCKER-A CHARMm-based MD docking algorithm. *J. Comput. Chem.* **24,** 1549–1562